



Science Arts & Métiers (SAM)

is an open access repository that collects the work of Arts et Métiers Institute of Technology researchers and makes it freely available over the web where possible.

This is an author-deposited version published in: <https://sam.ensam.eu>
Handle ID: <http://hdl.handle.net/10985/7658>

To cite this version :

Paola CINNELLA, Bruno MICHEL - Toward improved simulation tools for compressible turbomachinery: assessment of RBC schemes for the transonic NASA Rotor 37 benchmark case - In: Congrès français de mécanique (21 ; 2013 ; Bordeaux (Gironde))., France, 2013-08-26 - Congrès français de mécanique (21 ; 2013 ; Bordeaux (Gironde)). - 2013

Any correspondence concerning this service should be sent to the repository

Administrator : scienceouverte@ensam.eu



Toward improved simulation tools for compressible turbomachinery: assessment of RBC schemes for the transonic NASA Rotor 37 benchmark case

P. Cinnella[†], B. Michel[‡]

[†]. Laboratoire DynFluid, Arts et Métiers ParisTech, 151 Bd de l'Hôpital, 75013 Paris, France

[‡]. Département DSNA, Onera, 92320, Châtillon, France

Résumé :

Des schémas compacts basés sur le résidu (RBC) d'ordre 2 et 3 sont appliqués à un écoulement complexe 3D dans un compresseur transsonique. Les schémas proposés fournissent des solutions quasiment convergées en maillage et en bon accord avec les données expérimentales dans des maillages peu raffinés, ce qui permet une réduction du coût de calcul d'un facteur entre 2 et 4 par rapport aux solveurs classiques, pour un même niveau de précision.

Abstract :

Residual-based-compact schemes (RBC) of 2nd and 3rd-order accuracy are applied to a challenging 3D flow through a transonic compressor. The proposed schemes provide almost mesh-converged solutions in good agreement with experimental data on relatively coarse grids, which allows computational cost reductions by a factor between 2 and 4 with respect to standard solvers for a given accuracy level.

Mots clefs : Transonic compressor, Residual-Based compact scheme, high order

1 Introduction

The high complexity of turbomachinery flows, which are three-dimensional, unsteady, and often transitional, requires powerful computational tools and models. Numerical methods used in most of the currently available simulation codes, of nominal second order accuracy at most, often provide inaccurate results when applied to complex flow cases involving flow separation, shock waves and possible associated unsteadiness, unless very fine discretization grids are used. In an industrial context, the computational domain is often discretized by relatively coarse grids decomposed into several subdomains. In these conditions, the accuracy of classical numerical schemes, which is typically nominally second-order, may be decreased to first-order only. Nevertheless, numerical errors play an important role in the computation of turbomachinery performance. For instance, dissipative schemes and coarse meshes do not provide a correct description of vortex streets, which represent a substantial component of the blade profile losses. In this work, the capabilities of recently developed residual-based-compact scheme (RBC) of third-order accuracy are assessed for a challenging 3D compressible turbomachinery flow problem, namely, the Rotor 37 case. The NASA Rotor 37 is an isolated transonic axial flow compressor rotor with 36 blades. Extensive experimental data have been collected for this case with the aim of validating the predictive capabilities of numerical simulation codes. Experimental information includes the compressor characteristics at the nominal rotation speed, as well as radial distributions of the pressure ratio, temperature ratio, and adiabatic efficiency downstream of the blades for mass flow equal to 98% of the choke conditions.

Residual-Based Compact (RBC) schemes have been developed from some time now [1, 2, 4, 3] for computing multidimensional, inviscid and viscous, steady and unsteady, compressible flows. RBC schemes of 2nd and 3rd-order accuracy have been implemented within the structured multiblock finite

volume solver elsA [5] developed by the DSNA Department of ONERA [6]. Recent studies [7, 8] of the truncation error and spectral properties of unsteady RBC schemes have allowed to improve their stability and ensure robustness for any flow condition. This improved version has been recently extended to deformed curvilinear grids in a finite volume framework [9].

In the following, after providing the main features of the proposed numerical method, the Rotor37 configuration is calculated for several operating conditions in order to predict the rotor characteristics, and compare the results with the available experimental data and with those provided by the baseline solver available in elsA (Jameson's scheme) both in terms of accuracy and computational cost. Then, more in-detail analyses are carried out for a specific operating condition, corresponding to a mass flow equal to 98% the choked mass flow, for which experimental radial distributions of the rotor performance are available. Conclusions are drawn about the capabilities of RBC schemes of providing improved solutions in terms of accuracy, for a reduced computational cost compared to standard schemes.

2 Governing Equations and Residual-Based Compact approximation

In the present work, turbomachinery flows are modelled by the Reynolds-Averaged Navier-Stokes equations completed by a transport equation turbulence model. Precisely, the Spalart-Allmaras model is retained among different choices available in elsA [5], since it represents a good compromise among accuracy, computational cost, and numerical robustness. The main system of equations is approximated by means of a straightforward finite-volume extension of the RBC scheme of second-order accuracy (see [1, 6] for details), referred-to as RBC2, or by a mesh-weighted, high-order accurate finite volume extension of the RBC scheme of 3rd-order accuracy (see [9]), referred-to as RBC3. The last scheme makes use of weighted discretization operator, in order to ensure at least second-order accuracy on any deformed mesh, and third-order accuracy on smoothly deformed meshes. Details of the numerical schemes under investigation are omitted for brevity. The interested reader is referred to the cited references for further information. The turbulent transport equation is discretized by Roe's scheme with 3rd-order MUSCL extrapolation.

Being mainly interested into steady flow simulations, the steady version of RBC schemes is considered here. The solution is driven to the steady state by means of an implicit time-marching procedure. To reduce computational costs and preserve code modularity, a defect-correction strategy based on Roe-Harten implicit operator is adopted, solved by means of L-U factorisation.

3 Numerical simulation results

The NASA Rotor 37 is an isolated transonic axial compressor rotor with 36 blades. This case was initially included in a wider research program intended to cover a range of design parameters typical of aircraft turbine engine high-pressure compressor inlet stages. It has been presented in the AGARD Advisory Report n.355 [10] and used for the validation of CFD codes and turbulence models. All the data available for this case were measured with the Rotor operating at the equivalent design rotational speed of 17188.7 rpm. A total of 13 sets of overall performance data were measured between the choked mass flow (measured value $m_{\text{choke}} = 20.93$ Kg/s) and the stall flow rate (equal to 0.925 of the choke value, i.e. 19.36 Kg/s, according to experiments). Overall performance includes average total pressure ratio and adiabatic efficiency. Moreover, laser anemometer velocity data are also available for a mass flow rate of $0.98m_{\text{choke}}$.

Numerical computations were run using a series of three meshes made up by six structured blocks with conformal joins. The finest grid is clustered enough close to the walls so to be relevant for low-Reynolds computations. The coarsest grid uses values of y^+ greater than 10. The main properties of these meshes are given in Tab. 1. The medium and coarse grids are obtained through successive agglomerations of neighbouring cells (eight by eight) of the finest one. A view of the coarsest grid is provided in Fig. 1.

Boundary conditions base on local 1D Riemann invariants are used at inlet and outlet boundaries. At the inlet, total pressure and temperature, as well as flow direction are imposed. At the outlet, the static

TABLE 1 – Computational grids.

Grid	Cell count	Cell layers in the tip clearance	y^+
Fine	1 480 704	24	2
Medium	185 088	12	5
Coarse	23 136	6	15

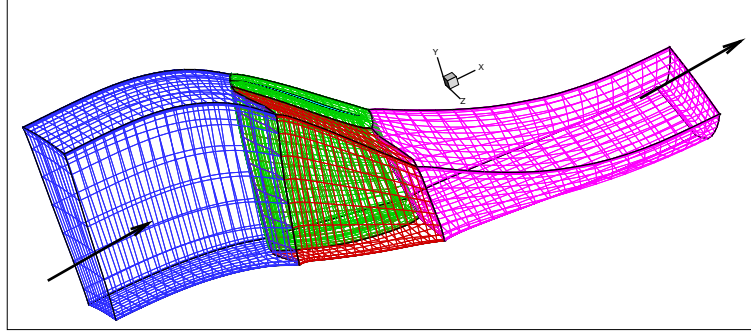


FIGURE 1 – View of the coarser grid.

pressure distribution (following radial equilibrium) is imposed and iteratively adjusted in order to achieve a prescribed target mass flow. The walls are assumed adiabatic. Numerical computations were carried out with a CFL number equal to 10 for all cases. Computations were stopped once the relative variation in mass flow rate was lower than 0.5%. A total of 5 operation points distributed along the compressor characteristic were computed on the two coarser grids, whereas only two operation points were computed with the finest grid. Figure 2 shows typical convergence histories of the continuity equation residual and of the non-dimensional mass flow rate on the finest mesh. Residuals drops about 4 orders of magnitudes, which is enough to reach the desired tolerance level on mass flow. Numerical solutions were post-treated in order to extract the overall performance parameters, namely the average total pressure ratio, P_{ratio} and the adiabatic efficiency η_{is} , defined as :

$$P_{ratio} = \frac{P_{t2}}{P_{t1}}; \quad \eta_{is} = \frac{\left(\frac{P_{t2}}{P_{t1}}\right)^{\frac{\gamma-1}{\gamma}} - 1}{\frac{T_{t1}}{T_{t2}} - 1}$$

where P_t and T_t represent respectively the total pressure and temperature in the absolute reference frame, and the subscripts 1 and 2 stand for inlet and outlet of the computational domain, respectively. Computed and experimental results for both quantities and displayed in Fig. 3. The RBC schemes tend to underestimate the pressure ratio and adiabatic efficiency in comparison to measurements. Results progressively improve when refining the mesh. An interesting result is that for RBC2 and, even more clearly, for RBC3, results obtained on the medium and fine grids are relatively close to each other, and to within 5% from experimental data, which may suggest that these schemes are close to mesh convergence. The coarse grid solution is very far from the fine mesh one, indicating that numerical errors are quickly reduced after the first grid refinement. On the contrary, the numerical solution provided by Jameson's scheme varies significantly with mesh refinement : the pressure ratio is strongly over-estimated on the coarser grid (and the choke mass flow under-estimated), becomes fortuitously close to experimental data after the first mesh refinement, and tends to be underestimated on the finest grid. Differences between the solutions obtained on the two last grids are quite significant, suggesting poor mesh convergence of the numerical solution.

To further investigate the impact of numerical approximations on the computed rotor performance, an in-detail analysis of the numerical flow fields was carried out for operating conditions corresponding to 98% of the choke mass flow. Figure 4 provides an overall view of the computed flow field provided by the RBC3 scheme on the finest grid. The flow field is characterised by a bow shock upstream of

the blade, as well as a passage shock leading to boundary layer separation. A complex shock structure is also present in the tip clearance. Figure 5 shows iso-Mach contours at the mid-plane computed on the finest grid with several schemes. Shock sharpness and size of the separation bubble vary according to the scheme in use : the sharpest shock and the greatest separation bubble are provided by RBC3, whereas Jameson's scheme tends to smear shocks and leads to a smaller separation bubble. Note also that the high-accurate scheme predicts a higher maximum value of the Mach number in the computational field : precisely, maximum values of 1.907, 1.844, and 1.828, are obtained for RBC3, RBC2, and Jameson's scheme, respectively.

Finally, Fig. 6 displays the radial distributions of rotor performance at an axial station located 10.67 cm downstream of the blade leading edge. For this station, experimental measurements of the radial distributions of total pressure ratio, total temperature ratio, and adiabatic efficiency are available. As recommended in [10], numerical solutions were mass-weighted in the azimuthal direction. As previously observed for overall performance indicators, numerical solutions provided by RBC schemes converge more quickly than Jameson's ones when the mesh is refined. RBC3 performs slightly better than RBC2, and provides results closer to experimental data, already on the medium grid. Also note that, already on the medium grid, RBC schemes capture well the dimple in Total pressure ratio distribution located around midspan. Jameson's solution on the coarser grids does not even follow the experimental trends. Similar remarks can be done on total temperature distributions. On the finer grid, the lower-order scheme captures the right trends, but the absolute values are less accurate than those of RBC schemes. Nevertheless, due to error compensation, the adiabatic efficiency distribution is rather good.

4 Conclusions

Numerical simulations of the Rotor37 test case are carried out at several operating conditions using RBC schemes of 2nd and 3rd-order accuracy. It is worthy stressing the novelty of computing such challenging complex flow fields using high accurate schemes. Comparisons of numerical solutions predicted by RBC schemes for increasing degrees of mesh resolution with those of the baseline solver in elsA, namely, Jameson's scheme, show that RBC schemes provide almost grid converged results on computational grids that are 8 times coarser. Thanks to the use of coarser grids, the use of RBC schemes reduces computational cost required to achieve mesh-converged solutions by a factor 2 to 4 compared to standard methods, even if their CPU cost per iteration and per point is 1.8 to 2.2 times higher. Specifically, if only steady computations are required, RBC2 provides the better compromise between accuracy, memory loading, robustness, and computational cost. On the other hand, two-dimensional unsteady computations [6] show that at least 3rd-order accuracy is required for unsteady computations. Numerical applications of RBC3 to unsteady 3D flows are warranted in the near future.

Références

- [1] Lerat A., Corre C. 2001 A Residual-Based Compact Scheme for the Compressible Navier-Stokes Equations. *J Comp Phys* **170** pp. 642-675
- [2] Lerat A., Corre C. 2002 Residual-based compact schemes for multidimensional hyperbolic systems of conservation laws. *Comp Fluids* **31** pp. 639-661
- [3] Lerat A., Corre C. 2006 Higher order residual-based compact schemes on structured grids. *34th Comput. Fluid Dyn. Course, von Karman Institute for Fluid Dynamics VKI LS 2006-1* pp. 1-111
- [4] Corre C., Hanss G., Lerat L. 2005 A residual-based compact scheme for the unsteady compressible Navier-Stokes equations *Comp Fluids* **34** pp. 561-580
- [5] <https://elsa.onera.fr>
- [6] Michel B., Cinnella P., Lerat A. 2011 Multiblock residual-based compact schemes for the computation of complex turbomachinery flows. *Int J Engin Sys Model Simulation* **3** pp. 2-15
- [7] Lerat A., Grimich K., Cinnella P. 2013 On the design of high order residual-based dissipation for unsteady compressible flows. *J Comp Phys* **235** pp. 32-51
- [8] Grimich K., Cinnella P., Lerat A. 2013 Spectral properties of high-order residual-based compact schemes for unsteady compressible flows. *J Comp Phys* **Submitted**
- [9] Grimich K., Michel B., Cinnella P., Lerat A. 2013 Generalized finite volume formulation of a third-order residual-based compact scheme for unsteady flow computations. *Comp Fluids* **Submitted**
- [10] AGARD Advisory Report AR-355 1998

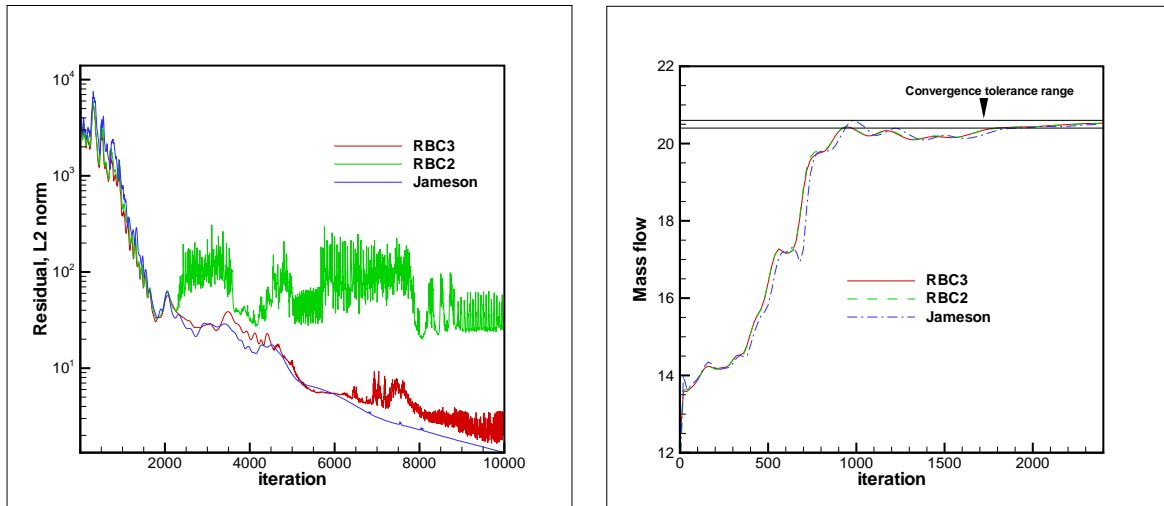


FIGURE 2 – Sample convergence histories, fine grid computation, 98% choke conditions.

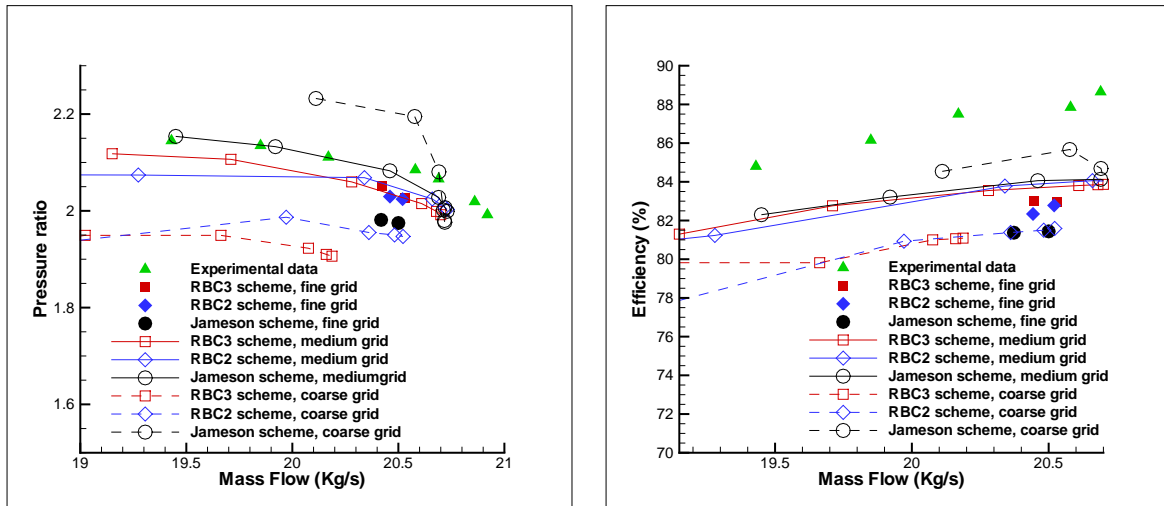


FIGURE 3 – Rotor37 compressor maps for several schemes and grid resolutions. Left : pressure ratio ; right : isentropic efficiency.

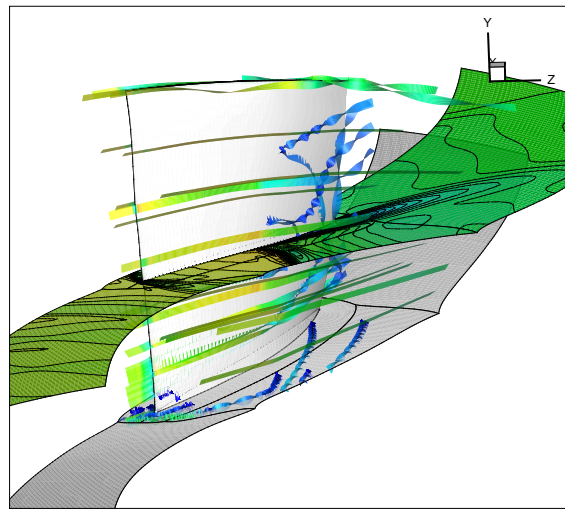


FIGURE 4 – Overall view of the flow field (98% choke conditions). Mach number distribution at midplane, and stream ribbons colored by the Mach number. RBC3 scheme.

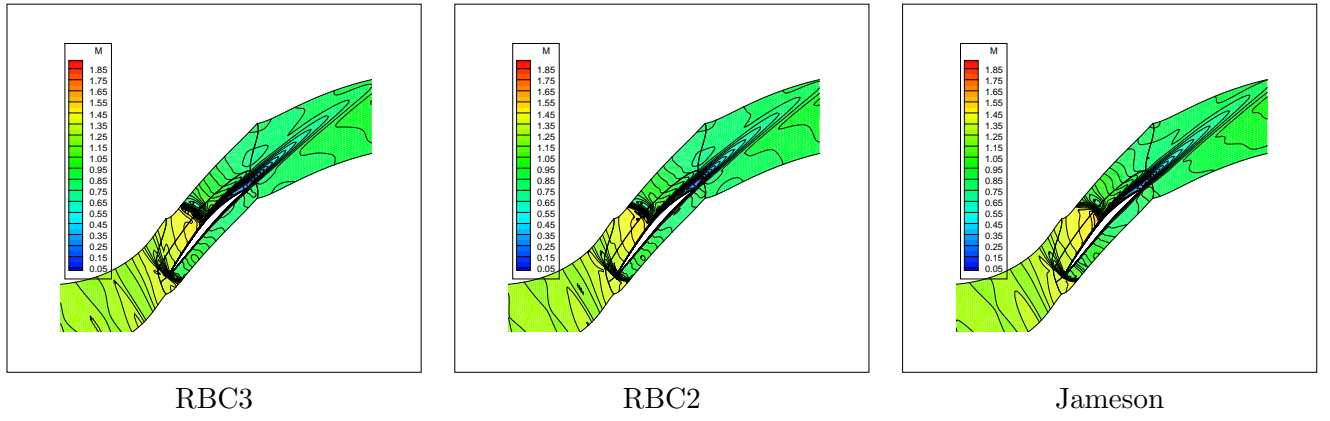


FIGURE 5 – Mach number distribution at compressor's midplane for several schemes. Fine grid computation.

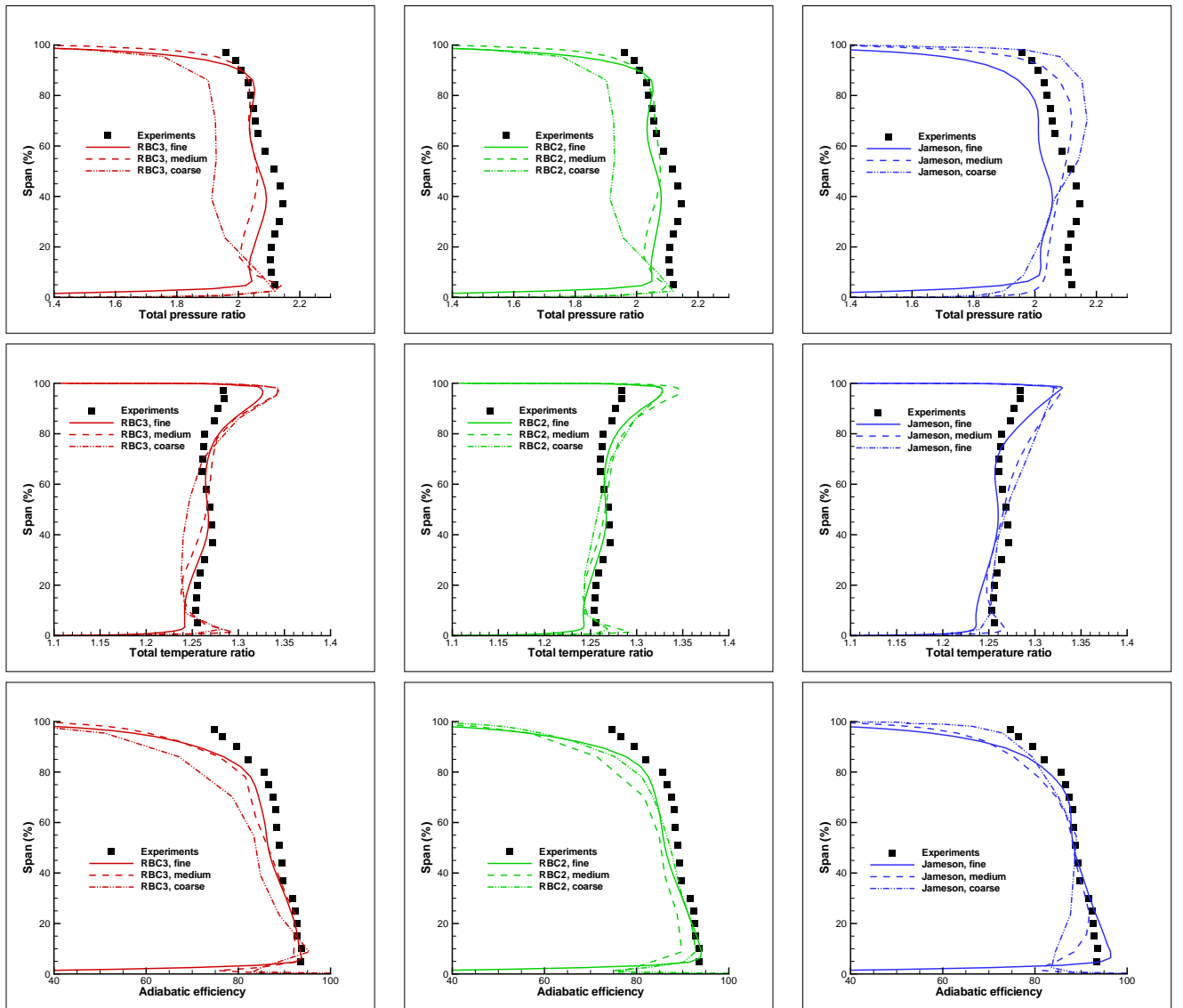


FIGURE 6 – Radial performance distributions for several schemes and grid resolutions.